

ENSO influence on Bay of Bengal cyclogenesis confined to low latitudes

Article

Published Version

Creative Commons: Attribution 4.0 (CC-BY)

Open Access

Roose, S. ORCID: <https://orcid.org/0000-0002-6444-4837>, Ajayamohan, R. S., Ray, P., Mohan, P. R. and Mohanakumar, K. (2022) ENSO influence on Bay of Bengal cyclogenesis confined to low latitudes. *npj Climate and Atmospheric Science*, 5. 31. ISSN 2397-3722 doi: 10.1038/s41612-022-00252-8 Available at <https://centaur.reading.ac.uk/130681/>

It is advisable to refer to the publisher's version if you intend to cite from the work. See [Guidance on citing](#).

To link to this article DOI: <http://dx.doi.org/10.1038/s41612-022-00252-8>

Publisher: Nature

All outputs in CentAUR are protected by Intellectual Property Rights law, including copyright law. Copyright and IPR is retained by the creators or other copyright holders. Terms and conditions for use of this material are defined in the [End User Agreement](#).

www.reading.ac.uk/centaur

CentAUR

Central Archive at the University of Reading

Reading's research outputs online

ARTICLE OPEN



ENSO influence on Bay of Bengal cyclogenesis confined to low latitudes

Shinto Roose^{1,2}, R. S. Ajayamohan^{1✉}, Pallav Ray³, P. Reshmi Mohan⁴ and K. Mohanakumar⁵

The low-latitude cyclones (LLCs, originating between 5°N–10°N) constitute ≈40% of tropical cyclones (TCs) formed in the Bay of Bengal (BoB). We investigate the interannual variability of post-monsoonal (October to December) BoB LLCs and their teleconnection with El Niño Southern Oscillation (ENSO) and Indian Ocean Dipole (IOD). It is found that the years with the fewer number of BoB LLCs are associated with anomalous equatorial easterlies that are largely connected with the El Niño and positive IOD. Likewise, equatorial westerly phases, often associated with the La Niña and negative IOD years, favour the LLC formation by providing the initial spin-up required for cyclogenesis. This teleconnection between ENSO/IOD and BoB TC frequency is confined in the low-latitude region with little influence for cyclogenesis north of 10°N during ENSO and IOD except during negative IOD. These results may help extend the lead time and improve the seasonal prediction of BoB TCs.

npj Climate and Atmospheric Science (2022)5:31 ; <https://doi.org/10.1038/s41612-022-00252-8>

INTRODUCTION

Tropical cyclones (TCs) in the Bay of Bengal (BoB) can cause substantial socio-economic damage and loss of life on densely populated coastal areas of the Indian subcontinent resulting from strong winds, storm surges, and heavy rainfall^{1–4}. The increasing coastal population has led to a significant increase in cyclone-related losses⁵. The major environmental factors that influence the genesis of TCs are the Coriolis parameter, relative vorticity, vertical wind shear, atmospheric stability, mid-tropospheric relative humidity, sea surface temperature (SST), and oceanic heat content^{6–9}. These environmental factors are favourable for TC genesis in the BoB during two seasons, viz., pre-monsoon (March–May) and post-monsoon (October–December)¹⁰. Depressions are active during the monsoon season (June–September), but TCs do not form quickly in a sheared-environment¹¹. The post-monsoon land-falling cyclones are devastating to the coastal areas of India and Bangladesh¹².

In the BoB, the TCs are categorised based on the maximum sustained wind (MSW)¹³ as the following: depression (17–27 knots), deep depression (28–33 knots), cyclonic storm (CS, 34–47 knots), severe cyclonic storm (SCS, 48–63 knots), very severe cyclonic storm (VSCS, 64–89 knots), extremely severe cyclonic storms (ESCS, 90–119 knots), and super cyclonic storm (SuCS, ≥120 knots). The maximum number of SCSs and higher categories occur during the post-monsoon season (Table 1)¹³.

Despite the basin-wide warming over the north Indian Ocean during the recent decades^{14–17}, the frequency of BoB cyclones has not increased significantly^{18,19}. The future projections consistently indicate that global warming will increase the intensity of TCs around the globe²⁰, including the BoB²¹. The intensity of SCS in the BoB during the post-monsoon season has increased from 1981 to 2010²². A notable increase in frequency and duration of VSCS in the north Indian Ocean is reported during 1981 to 2014²³. In addition, the genesis locations of VSCSs in the BoB have shifted eastward by around 2°, suggesting an increase in storm duration in recent years²³. A significant growing trend in the annual

frequency of VSCS in the Arabian Sea is documented during 1982 to 2019, although no significant trend in the BoB was detected¹⁹. The amount of energy disbursed by the BoB cyclones has also increased in recent decades²⁴.

Apart from these long-term and seasonal changes in the BoB TC frequency, they also exhibit pronounced interannual variability related to natural climate modes. The SST anomalies in the equatorial Pacific during El Niño Southern Oscillation (ENSO)^{25–27} events can remotely influence other oceans through Walker Circulation²⁸. Similarly, the tropical Indian Ocean has a basin-wide variability termed the Indian Ocean Dipole (IOD)²⁹. These two leading modes (ENSO and IOD) influence the interannual variability of BoB TCs^{3,30–34}. La Niña and negative IOD events are favourable for the severe cyclone activities in the BoB during the post-monsoon season³¹.

The leading climate modes like ENSO and IOD modulate the ocean-atmosphere conditions in different latitudes of the BoB contrarily. This, in turn, influences the TC genesis differently at different latitudes. Hence, the primary goal of this study is to understand the interannual variability in BoB-TCs at low (5°–10°N) and high (>10°N) latitudes that are modulated by ENSO and IOD. Past studies on ENSO/IOD teleconnection with the BoB TCs^{31,32} considered the TC variability in the entire BoB. As a result, they may have missed the disparate changes in TC frequency with latitudes. In this study, we show that ENSO/IOD influence is confined to changes in the frequency of low-latitude cyclones (LLCs, formed between 5°–10°N) only, with no significant changes in the frequency of high-latitude cyclones (HLCs, formed north of 10°N) during contrasting phases of ENSO and IOD except during negative IOD.

RESULTS AND DISCUSSION

Interannual variability of the Bay of Bengal LLCs and HLCs

During 1979–2020, out of 167 TCs formed in the north Indian Ocean, 48 formed in the Arabian Sea, and 119 formed in the BoB

¹Center for Prototype Climate Modeling, New York University, Abu Dhabi, UAE. ²Department of Atmospheric Sciences, Cochin University of Science and Technology, Kochi, India. ³Meteorology, Ocean Engineering and Marine Sciences, Florida Institute of Technology, Melbourne, FL, USA. ⁴Abu Dhabi Polytechnic, Institute of Applied Technology, Abu Dhabi, UAE. ⁵Advanced Centre for Atmospheric Radar Research, Cochin University of Science and Technology, Kochi, India. ✉email: Ajaya.Mohan@nyu.edu

Table 1. Seasonal and annual frequency of TCs formed in the Arabian Sea, Bay of Bengal, and the entire north Indian Ocean during 1979–2020.

Season	Arabian Sea	Bay of Bengal	North Indian Ocean
Jan–Feb	0 (0)	4 (1)	4 (1)
Mar–May	9 (5)	27 (19)	36 (24)
Jun–Sep	16 (11)	11(2)	27 (13)
Oct–Dec	23 (15)	77 (48)	100 (63)
Annual	48 (31)	119 (70)	167 (101)

The number of TCs intensified into Severe Cyclonic Storms (SCS), and higher categories are listed in parentheses.

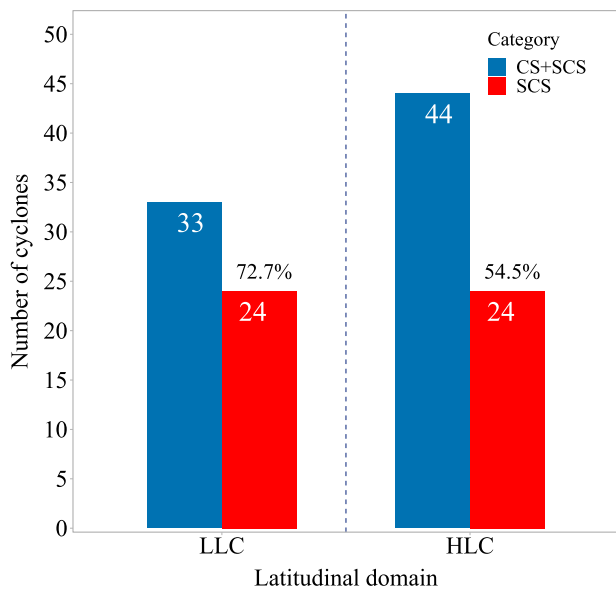


Fig. 1 Statistics of post-monsoon season Bay of Bengal cyclones during 1979–2020. Number of cyclonic storms (CS) and severe cyclonic storms (SCS) formed over the low latitudes (LLC, originating between 5°N and 10°N) and high latitudes (HLC, originating north of 10°N).

(Table 1). The BoB is conducive for TC formation during the pre- and post-monsoon seasons and accounts for 71% of the north Indian Ocean cyclones (Table 1). Out of all post-monsoon cyclones in the BoB, 33 (43%) of them were formed over the low latitudinal region (5°–10°N), and 44 (57%) formed over the north of 10°N (Fig. 1). Out of the 33 LLCs, 24 (73%) further intensified into SCSs, likely due to their longer travel time over water, whereas out of 44 HLCs, only 24 (55%) intensified into SCSs (Fig. 1).

The statistics of LLC and HLC frequency and its teleconnection with ENSO/IOD modes are given in Table 2. Based on the oceanic El Niño index²⁶, there were 12 El Niño and 11 La Niña years during 1979–2020. During El Niño years, the average number of HLCs is the same as its climatological mean (≈ 1 TC per year). In contrast, the average LLC number during El Niño years is reduced by 58% (0.33) from its climatological mean (0.79, Table 2). In comparison, the LLC frequency is increased by 38% during the La Niña years. On average, the frequency of LLCs and HLCs is the same during the La Niña years (Table 2). Although a 27% decrease in TC frequency during El Niño years and a 19% increase during La Niña years are visible in the total TCs formed over the BoB, the corresponding percentage departures are more in the LLCs (–58% and +38%, Table 2).

Similarly, based on the dipole mode index (DMI)²⁹ during the IOD peak season (September–November), there were 11 positive and 9 negative IOD years during the analysis period. The average frequency of LLC dropped by 42% during positive IOD years and increased by 41% during negative IOD years. The interannual variability in the frequency of LLCs is much more visible and significant than the frequency of the total TCs and HLCs developed over the BoB. The frequency of LLCs during El Niño and positive IOD years is fewer than the climatological mean. On the contrary, the frequency of BoB LLCs is higher than the climatological mean during La Niña and negative IOD years. The average number of HLCs during all categories of ENSO and IOD years does not vary much (close to the climatological mean) except for negative IOD years, when the frequency of HLCs is increased by 38% from its climatological mean (Table 2). Although the frequency of LLCs shows association with ENSO and IOD variability, the intensity of LLCs does not show significant teleconnection. Around 70–83% LLCs have intensified into SCSs and higher categories considering all phases of ENSO and IOD (Fig. 2). However, only 50–67% HLCs have intensified into SCSs and higher categories (Fig. 2). Consistent with previous studies³¹, the frequency of TCs in the BoB is higher during La Niña years and fewer during El Niño years (Fig. 2 and Table 2). However, the HLC frequency barely changed during the contrasting phases of the ENSO. For example, the average number of HLC remains the same (≈ 1 TC per year) for La Niña and El Niño (Table 2). On the other hand, the frequency of LLCs of ≈ 1 TC (per year) during La Niña has declined to ≈ 0.3 TC (per year) during El Niño (Table 2). A similar relationship is found for severe cyclonic storms (SCS), where the changes in TC frequency are dominant in the low latitudes (Fig. 2). Hence, the change in TC frequency in the BoB during different phases of El Niño is dominated by the change in the low latitudinal regions. Overall, this analysis clearly shows that the reduction in TC frequency during El Niño and increase in TC frequency during La Niña is almost entirely due to changes in LLC frequency. For different phases of IOD, there is a change in HLC frequency as well, but the change in LLC frequency is more prominent (Fig. 2 and Table 2). This observation motivates us to find the underlying causes behind such latitudinal contrasts.

Environmental conditions responsible for interannual variability of LLCs

To explore the interannual variability in TC frequency in BoB, we analyse the critical environmental parameters that influence cyclogenesis during contrasting ENSO (Fig. 3) and IOD (Fig. 4) years. The anomalous SST does not show any significant difference during El Niño (Fig. 3a) or La Niña (Fig. 3b) years over the LLC genesis region (black rectangular box in Fig. 3). The SST over the LLC genesis region is 28.5°–29°C (Fig. 5a), which is warmer than the critical SST (26°C) needed for supporting TC genesis⁸. The decline in the LLC frequency during El Niño (Table 2) cannot be attributed to an increase in SST. The tropical cyclone heat potential (TCHP)³⁵, is another ocean parameter important for the cyclone genesis and intensification, which has been increasing along the Indian coastline over BoB¹⁹. During the El Niño years, the mean TC genesis position in the BoB shifts westward, whereas eastern BoB experiences more TCs during the La Niña years, attributed to the ENSO-related changes in TCHP³¹. The change in TCHP over the LLC region is not significant during the contrasting phases of ENSO (Fig. 3c, d).

A mid-tropospheric relative humidity of 50–60% is often needed for the formation of cyclones to keep an air parcel saturated during ascent^{8,36}. The mid-tropospheric (700 hPa) relative humidity also increases over the genesis region of LLC during El Niño years (Fig. 3e), which cannot support a reduction in the LLC frequency. The vertical wind shear (between 200 and 850 hPa) in the low latitudinal region is significantly weak during

Table 2. Statistics of post-monsoon season (OND) Bay of Bengal cyclones during contrasting phases of ENSO and IOD during 1979–2020.

Year	Total BoB TC (per year)	LLC (per year)	HLC (per year)
All Years	1.83 (77TC/42yrs)	0.79 (33TC/42yrs)	1.05 (44TC/42yrs)
El Niño	1.33 (16TC/12yrs) ↓27%	0.33 (04TC/12yrs) ↓58%	1.00 (12TC/12yrs) ↓5%
La Niña	2.18 (24TC/11yrs) ↑19%	1.09 (12TC/11yrs) ↑38%	1.09 (12TC/11yrs) ↑4%
Neutral ENSO	1.95 (37TC/19yrs) ↑6%	0.89 (17TC/19yrs) ↑13%	1.05 (20TC/19yrs) ↑0%
PIOD	1.45 (16TC/11yrs) ↓21%	0.45 (05TC/11yrs) ↓42%	1.00 (11TC/11yrs) ↓5%
NIOD	2.55 (23TC/09yrs) ↑40%	1.11 (10TC/09yrs) ↑41%	1.44 (13TC/09yrs) ↑38%
Neutral IOD	1.72 (38TC/22yrs) ↓6%	0.82 (18TC/22yrs) ↑4%	0.91 (20TC/22yrs) ↓13%
Normal Years	1.73 (19TC/11yrs) ↓6%	0.82 (09TC/11yrs) ↑4%	0.91 (10TC/11yrs) ↓13%

The number of TCs that are formed over the low latitudes (LLC, formed between 5°N–10°N) and high latitudes (HLC, formed north of 10°N) are explicitly listed. The up and down arrows indicate the increase and decrease (%) in cyclone frequency from their climatological mean listed in the first row. The “Normal Years” do not include +ve/–ve IOD/ENSO years.

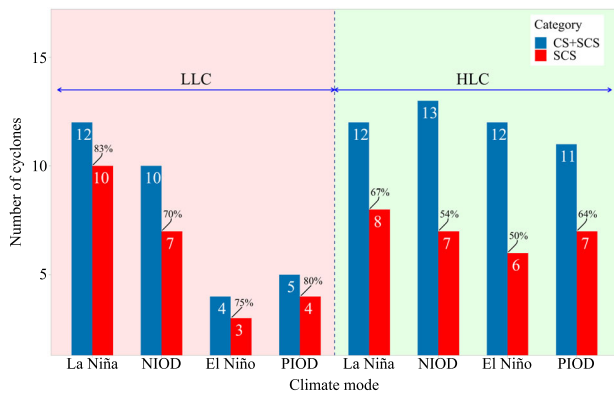


Fig. 2 Statistics of post-monsoon season Bay of Bengal cyclones during El Niño (La Niña) and positive IOD (negative IOD) years (1979–2020). Number of cyclonic storms (CS) and severe cyclonic storms (SCS) formed over the low latitudes (LLC, originated between 5°N–10°N) and high latitudes (HLC, originated in a latitude >10°N) during El Niño, La Niña, positive IOD (PIOD) and negative IOD (NIOD) years.

El Niño years (Fig. 3g). This reduced wind shear ($\approx 6 \text{ ms}^{-1}$, Fig. 5c) is favourable for TC genesis since a wind shear of $<10 \text{ ms}^{-1}$ is often considered supportive for TC development³⁷. Therefore, low vertical wind shear during El Niño years may not limit LLC development.

The other critical factor for cyclogenesis at the low latitudes is relative vorticity³⁸. The ambient rotation (i.e., small Coriolis) is insignificant at the low latitudes. Once a storm forms in the low latitudes under a lower planetary vorticity environment, it can spin-up faster and develop rapidly into cyclonic intensity than in higher latitudes with a higher Coriolis parameter environment^{39,40}. This is because the air in the boundary layer can penetrate closer to the storm centre over a weak planetary vorticity environment⁴¹. The El Niño composites show weakened relative vorticity anomalies compared to the climatological mean (Fig. 3i), supporting a reduction in LLC frequency (Table 2 and Fig. 2).

During La Niña years, no significant change in the SST (Fig. 3b), TCHP (Fig. 3d) and mid-tropospheric relative humidity (Fig. 3f) anomalies were observed over the low latitudinal region of the BoB. Both SST and mid-tropospheric relative humidity during La Niña years are smaller than El Niño years (Fig. 5a, b). There is an anomalous increase in vertical wind shear over low latitudes during La Niña years (Fig. 3h) compared to a decrease during El Niño years (Fig. 3g), which is also not favourable for LLC formation during La Niña years. Contrary to El Niño composites, the anomalous relative vorticity is increased

significantly over the low latitudes during the La Niña years (Fig. 3i, j). The increase in relative vorticity enhances the initial spin-up for the formation of LLCs in a weak planetary vorticity environment during La Niña years.

Similar conditions of El Niño and La Niña years occur during positive and negative IOD years. There is a significant increase in SST and mid-tropospheric relative humidity in the genesis location of LLCs during positive IOD years (Fig. 4a, e). The average values of SST ($\approx 28.75^\circ\text{C}$, Fig. 5a) and the relative humidity (65%, Fig. 5b) are greater than their critical values for the formation of TCs, while the LLCs are noticeably fewer. As in the case of El Niño, TCHP increases over a small portion of the western half of the LLC genesis region during positive IOD years (Fig. 4c). The vertical wind shear in the low latitudes of BoB is reduced (Fig. 4g) during positive IOD years. The vertical wind shear of $<10 \text{ ms}^{-1}$ facilitates intensification of TCs, and values between 2 and 4 ms^{-1} favour significant intensification³⁷. Therefore, the average vertical wind shear value of 6 ms^{-1} over the genesis region of BoB LLC (Fig. 5c) during positive IOD years does not inhibit TC intensification. In a weak planetary vorticity environment, relative vorticity is the major factor for cyclogenesis. The weak lower tropospheric vorticity in the LLC genesis location during positive IOD (see Fig. 4i and Fig. 5d) reduces the LLC frequency (Table 2).

During negative IOD years, the SST and mid-tropospheric relative humidity decreases over the low latitudinal region of the Bay of Bengal (Fig. 4b, f). However, the average values of the SST and mid-tropospheric relative humidity (28.5°C and 65%, Fig. 5a, b) are greater than their critical values for the formation of TCs. The TCHP significantly increases only over a small portion of the eastern half of the domain (Fig. 4d).

The vertical wind shear values $>11 \text{ ms}^{-1}$ favour significant weakening of TC³⁷. Even though the average vertical wind shear during negative IOD composite is 12 ms^{-1} (Fig. 5c), the number of LLCs is more than the climatological mean (Table 2 and Fig. 2). The increased LLCs during negative IOD years can be attributed to the increased vorticity (Figs. 4j and 5d). It is, therefore, evident that the relative vorticity plays a significant role compared to the other parameters responsible for TC genesis in the low latitudinal BoB.

The distinct behaviour of the factors responsible for cyclogenesis of LLCs and HLCs during the contrasting phases of ENSO and IOD is explored further. For example, the composite analysis reveals that the signs of mid-tropospheric relative humidity and vertical wind shear anomalies flip during positive/negative phases of ENSO and IOD (see Fig. 3e–h) and Fig. 4e–h). The mean SSTs over LLC and HLC formation region during positive/negative phases of ENSO/IOD events are high ($\approx 28.5^\circ\text{C}$) and sufficient for TC genesis (Fig. 5a). Compared to the HLC genesis region, higher mid-tropospheric relative humidity in the LLC genesis region (Fig. 5b) can support

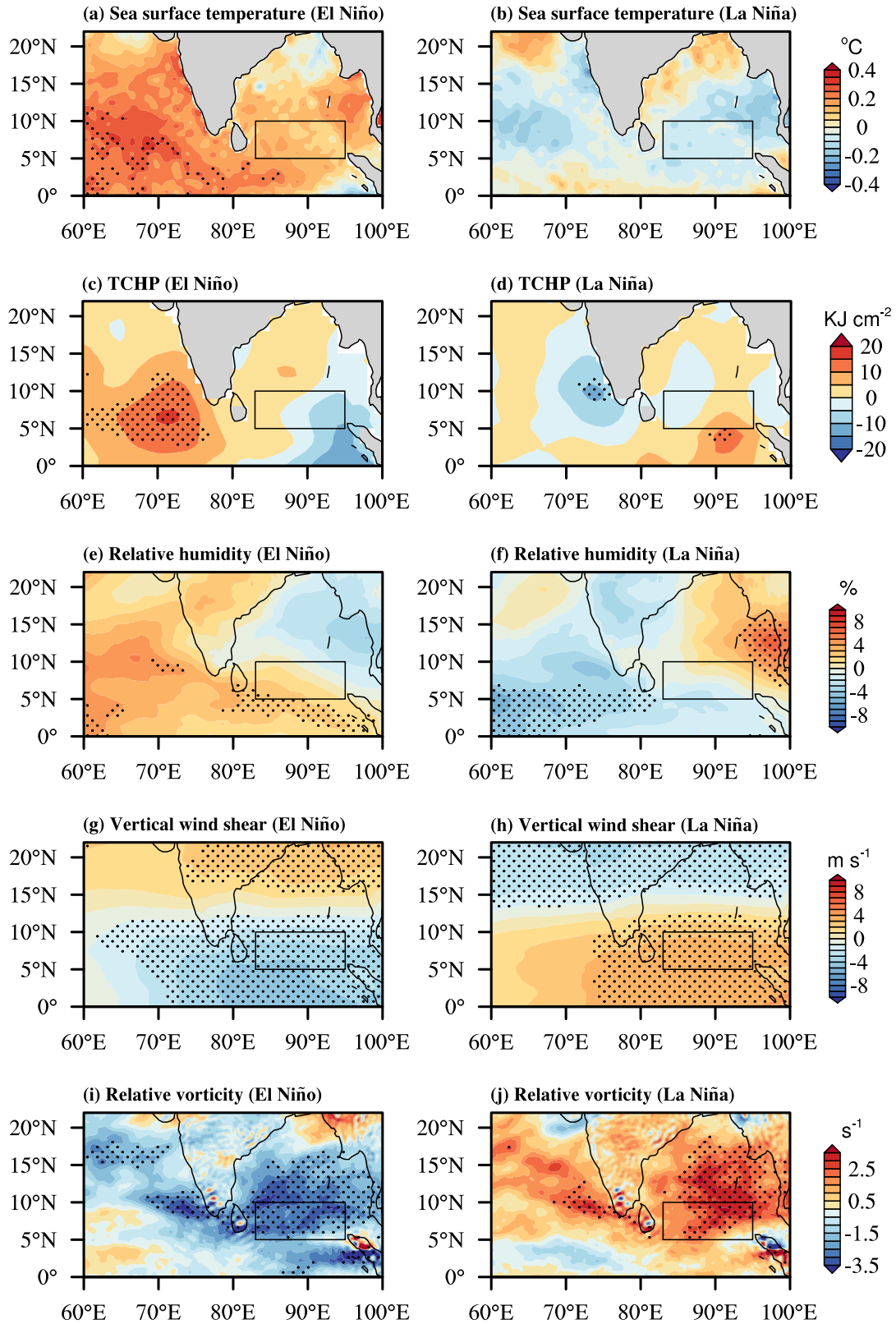


Fig. 3 El Niño and La Niña composites of critical environmental parameters that influence cyclogenesis. El Niño and La Niña composites of anomalous **a, b** sea surface temperature ($^{\circ}\text{C}$), **c, d** tropical cyclone heat potential (TCHP, KJcm^{-2}), **e, f** mid-tropospheric (700 hPa) relative humidity (%), **g, h** vertical wind shear between 850 and 200 hPa (ms^{-1}), and **i, j** low-level (850 hPa) relative vorticity ($\times 10^{-6}\text{s}^{-1}$). Stippled areas represent regions where anomalies are significant at the 95% confidence level. The genesis location of BoB LLCs is indicated by the black rectangular area ($83^{\circ}\text{--}95^{\circ}\text{E}$, $5^{\circ}\text{--}10^{\circ}\text{N}$).

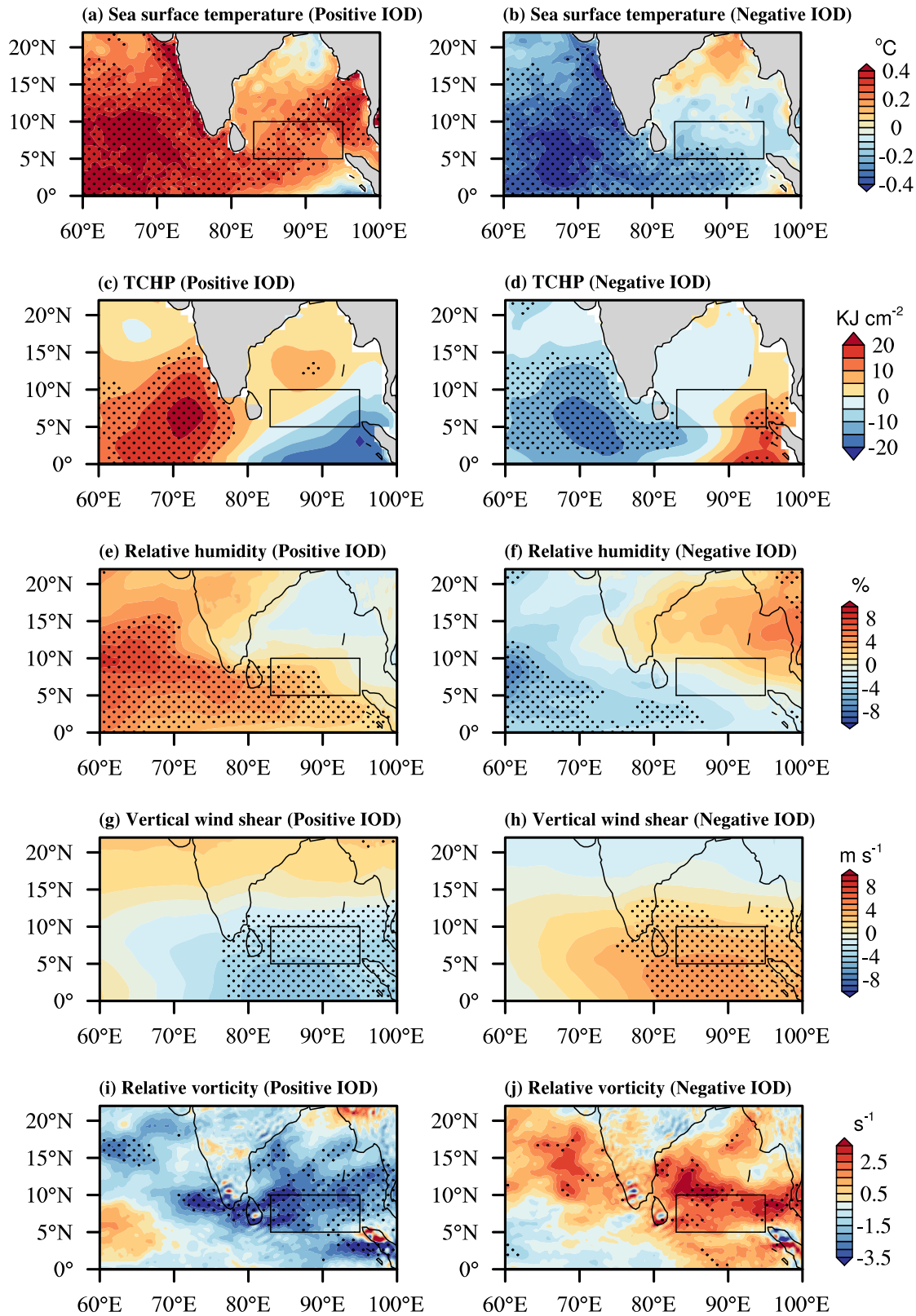


Fig. 4 Positive IOD and negative IOD composites of anomalous. **a, b** Sea surface temperature ($^{\circ}\text{C}$), **c, d** tropical cyclone heat potential (TCHP, KJcm^{-2}), **e, f** midtropospheric (700 hPa) relative humidity (%), **g, h** vertical wind shear between 850 and 200 hPa (ms^{-1}), and **i, j** low-level (850 hPa) relative vorticity ($\times 10^{-6} \text{ s}^{-1}$). Stippled areas represent regions where anomalies are significant at the 95% confidence level. The genesis location of BoB LLCs is indicated by the black rectangular area ($83^{\circ}\text{--}95^{\circ}\text{E}$, $5^{\circ}\text{--}10^{\circ}\text{N}$).

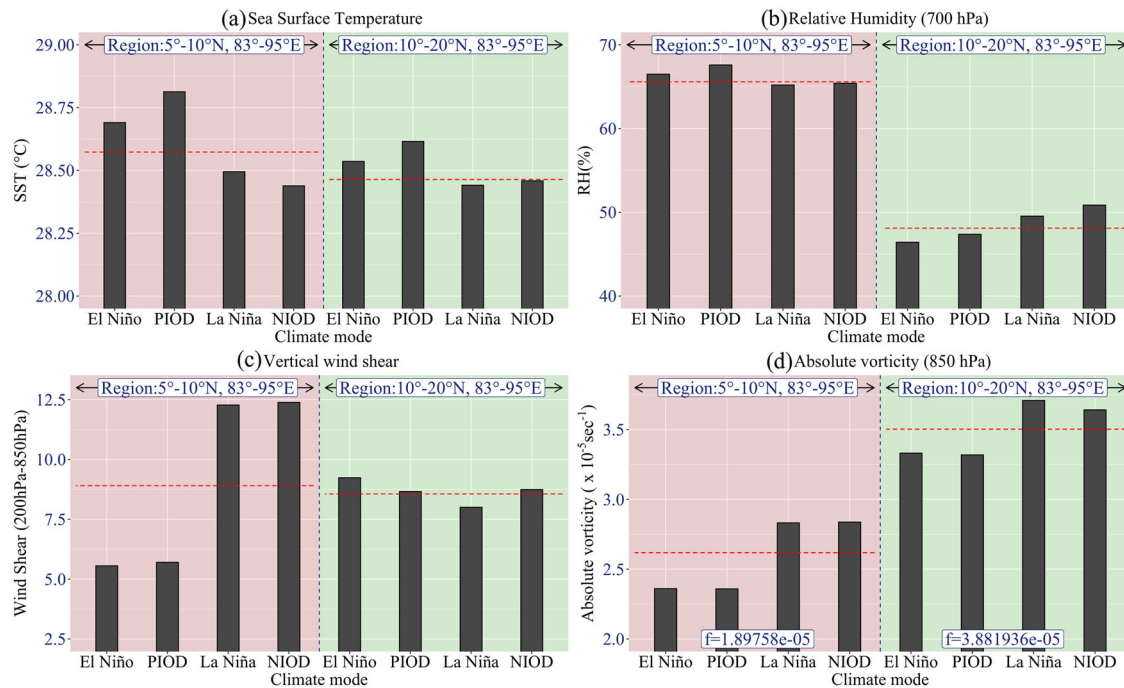


Fig. 5 Area-average of critical environmental parameters that influence cyclogenesis over the genesis region. **a** sea surface temperature (°C), **b** mid-tropospheric (700 hPa) relative humidity (%), **c** vertical wind shear between 850 and 200 hPa (ms^{-1}), and **d** low-level (850 hPa) absolute vorticity ($\times 10^{-5} \text{sec}^{-1}$) averaged over the low latitudinal genesis region ($5^{\circ}\text{--}10^{\circ}\text{N}$, $83^{\circ}\text{--}95^{\circ}\text{E}$, under red shades), and high latitudinal genesis region ($10^{\circ}\text{--}20^{\circ}\text{N}$, $83^{\circ}\text{--}95^{\circ}\text{E}$, under green shades) during the contrasting phases of ENSO and IOD. The horizontal dashed lines indicate the mean values of cyclogenesis parameters in LLC and HLC genesis region.

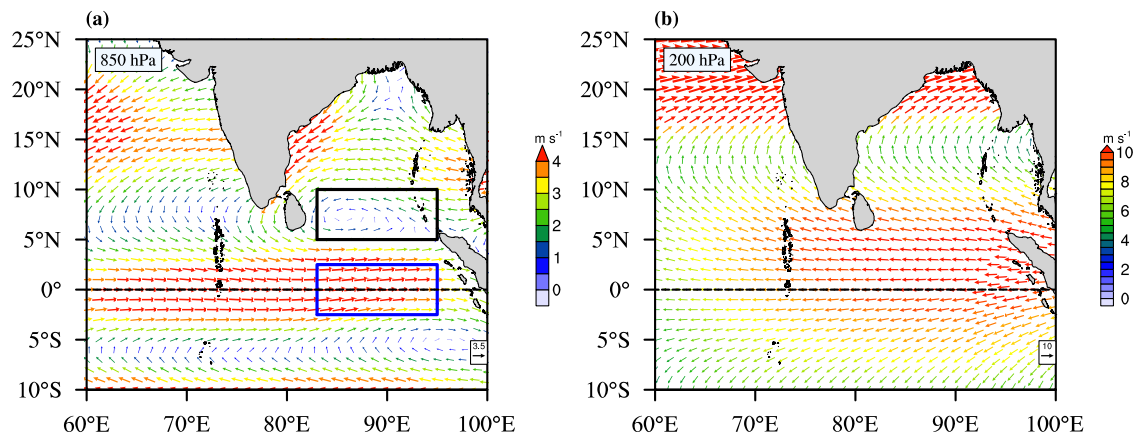


Fig. 6 Mean winds (ms^{-1}) during the post-monsoon season (1979–2020). Winds at **a** 850 hPa, and **b** 200 hPa. The colour bars represent the magnitude of wind. The black rectangular area ($83^{\circ}\text{--}95^{\circ}\text{E}$, $5^{\circ}\text{--}10^{\circ}\text{N}$) denotes the genesis location of BoB LLCs, and the blue rectangle ($83^{\circ}\text{--}95^{\circ}\text{E}$, $2.5^{\circ}\text{S}\text{--}2^{\circ}5\text{N}$) denotes the area over which equatorial winds are considered.

intensification of LLCs (Fig. 2). The average mid-tropospheric relative humidity over the LLC region is above 65% (Fig. 5b, red shading). The HLC region has a weak mid-tropospheric relative humidity of about 48% (Fig. 5b, green shading). Although the vertical wind shear over the LLC region shows a significant difference between positive and negative phases of ENSO/IOD, the vertical wind shear over the HLC region remains close to its climatological mean ($\approx 9 \text{ms}^{-1}$, Fig. 5c).

Even though relative vorticity reduces significantly over the LLC and HLC regions during El Niño (Fig. 3i) and positive IOD years (Fig. 4i), the decline in TC frequency is confined only in the low-latitude region (Table 2) due to the weak Coriolis force (Fig. 5d). This indicates the quintessential role of relative vorticity compared to the other parameters during the contrasting phases

of ENSO and IOD, especially over the genesis location of LLC (boxed region in Figs. 3i, j and 4i, j). To confirm that the decrease in relative vorticity during El Niño/positive IOD years and its increase during La Niña/negative IOD years was not due to the TC-related circulation anomalies, we removed TC-related anomalies from the basic flow⁴². The results still show reduced relative vorticity during El Niño/positive IOD and enhanced relative vorticity during La Niña/negative IOD over the LLC region (Supplementary Figs. 1 and 2).

Dependence of LLCs on equatorial winds

To understand the formation of unfavourable vorticity pattern for LLC genesis during El Niño and favourable pattern during La Niña years, we examined the seasonal mean low-level winds.

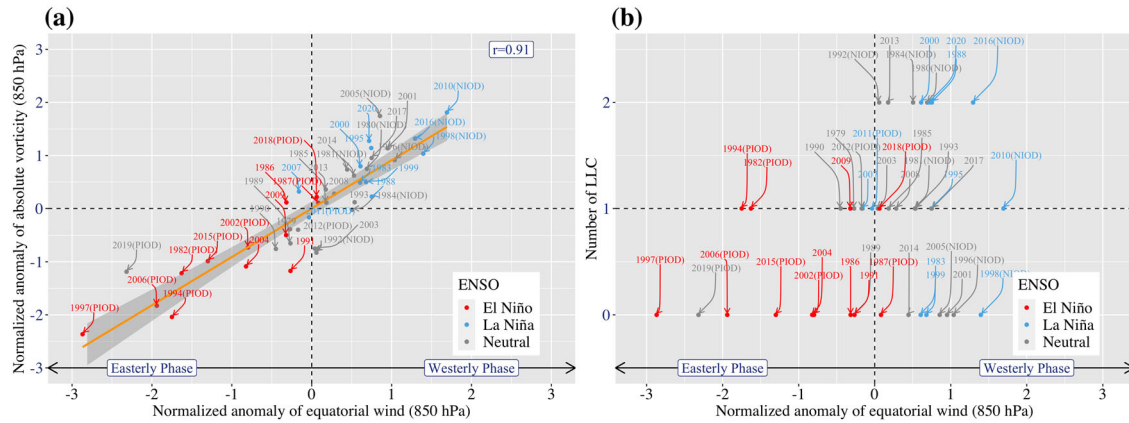


Fig. 7 The relationship between equatorial wind anomalies, low-level absolute vorticity, and BoB LLC frequency during contrasting phases of ENSO. **a** Equatorial wind anomalies versus 850hPa absolute vorticity, and **b** Equatorial wind anomalies versus BoB LLC frequency. Both equatorial wind anomalies (averaged over 2.5°S–2.5°N, 83°E–95°E) and absolute vorticity anomaly (averaged over 5°S–10°N, 83°E–95°E) are normalised by its own standard deviation. The El Niño, La Niña and neutral ENSO years are marked in red, blue, and grey colours, respectively. Years are labelled using arrows to the points. The linear trend is shown as the orange line, and the grey shading indicates 95% confidence level in panel **a**. During El Niño and positive IOD years, equatorial westerlies weaken leading to reduced absolute vorticity and fewer number of LLCs. The reverse occurs during La Niña and negative IOD years.

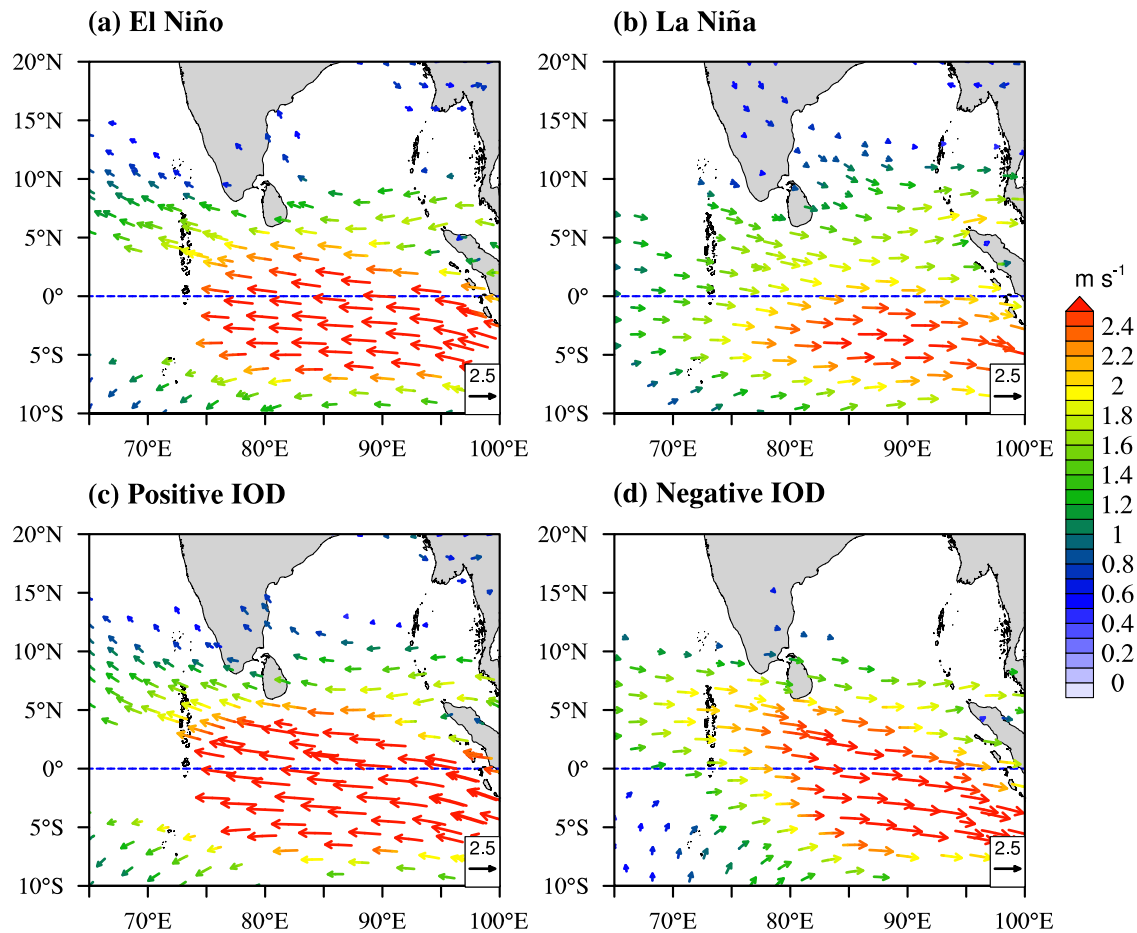


Fig. 8 Composite of 850hPa wind anomalies (ms^{-1}). **a** El Niño, **b** La Niña, **c** positive IOD, and **d** negative IOD years. Only statistically significant (95% confidence level) anomalies are shown.

The climatological mean winds (Fig. 6) splash a cyclonic gyre over the low-latitude region (5°–10°N) of the BoB during the post-monsoon season. We investigate how the contrasting ENSO/IOD phases modulate this cyclonic gyre since such a gyre can provide an initial spin-up for LLCs to form.

The equatorial winds (over the blue rectangular box in Fig. 6a) at 850 hPa strongly correlate with the absolute vorticity ($r = 0.91$) in the LLC region (black rectangular box in Fig. 6a) of BoB during the post-monsoon season (Fig. 7a). Most of the El Niño events fall in quadrant-III, while most La Niña events fall in quadrant-I in

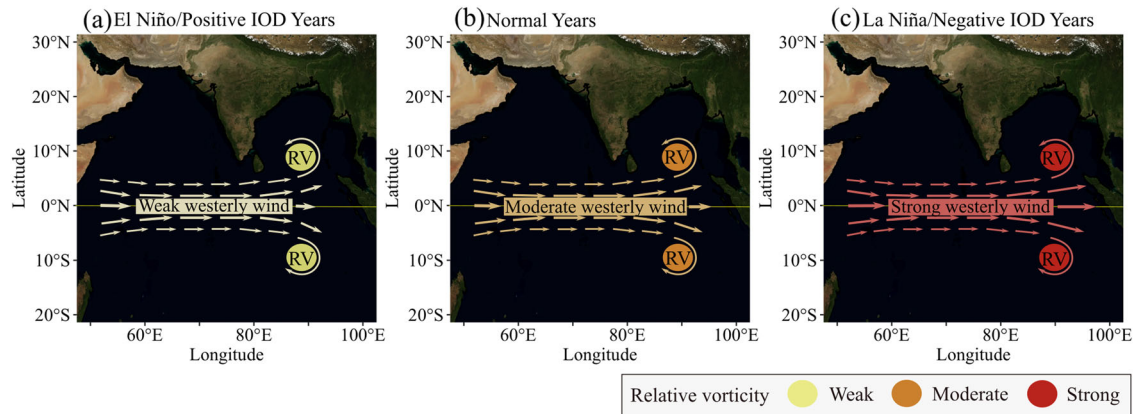


Fig. 9 Schematic representation of the interplay between low-level equatorial winds and relative vorticity anomalies during ENSO and IOD phases. Panel **a** shows the weak low-level relative vorticity on either side of the equator induced by weak equatorial westerly winds during El Niño/positive IOD years compared to normal years represented in panel **b**. Enhancement in the relative vorticity induced by strong westerly winds during La Niña and negative IOD years is depicted in panel **c**. The satellite image extracted from the Blue Marble Next Generation, NASA's Earth Observatory is used as basemap.

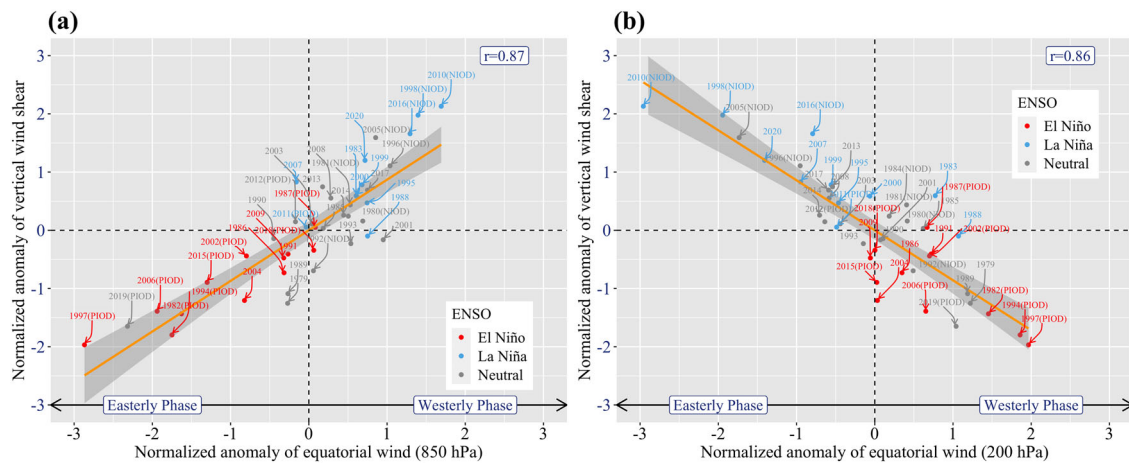


Fig. 10 The relationship between equatorial winds and vertical wind shear. **a** 850hPa equatorial wind anomalies versus vertical wind shear, and **b** 200hPa equatorial wind anomalies versus vertical wind shear. While the vertical wind shear anomalies are averaged over 5°N–10°N, 83°E–95°E, the equatorial wind anomalies are averaged over 2.5°S–2.5°N, 83°E–95°E. All variables are normalised by its own standard deviation. The El Niño, La Niña and neutral ENSO years are marked in red, blue and grey colours, respectively. Years are labelled using arrows to the points. The linear trend is shown as the orange line, and the grey shading indicates 95% confidence level.

Fig. 7a). It turns out that 83% of El Niño events are associated with the easterly phase of equatorial winds (Fig. 7a), and the rest are associated with very weak westerly winds. On the other hand, 82% of La Niña events are associated with the westerly phase of equatorial winds (Fig. 7a). In addition, 82% of the positive IOD years are associated with easterly phases of equatorial winds (Fig. 7a). In contrast, all negative IOD years in the analysis period are associated with the westerly phases. In a nutshell, fewer LLCs are associated with the easterly phases of equatorial winds during El Niño and positive IOD. In contrast, a higher number of LLCs are associated with the westerly phases during La Niña and negative IOD events (Fig. 7b).

The climatological westerly winds (Fig. 6a) in the equatorial Indian Ocean weaken during the El Niño and positive IOD years (Fig. 8a, c). This weakened westerly winds (Fig. 8a, c) during El Niño and positive IOD events reduce the absolute vorticity (Figs. 3i, 4i and 7a), which in turn affects the LLC genesis in the BoB. During the post-monsoon seasons of La Niña and negative IOD years, the anomalous equatorial westerly winds (Fig. 8b, d) increase the absolute vorticity over the low latitudes of the BoB (Figs. 3j, 4j and 7a). This increase in the absolute vorticity associated with stronger

equatorial westerlies (Fig. 7a) enhances the formation of LLCs (Fig. 7b). The role of equatorial winds in generating relative vorticity is summarised in a schematic (Fig. 9).

Even though the relative vorticity plays a decisive role in LLC formation, the vertical wind shear also varies with the contrasting phases of ENSO and IOD. We further explored the reason behind changes in vertical wind shear over the low latitudinal region during opposite phases of ENSO/IOD. Climatologically, equatorial westerlies prevail in the lower troposphere, and easterlies stay in the upper troposphere during post-monsoon months (Fig. 6). Both the lower-level (850 hPa) westerlies and upper-level (200 hPa) easterlies weaken during El Niño and positive IOD years (Fig. 10), resulting in the weakening of the vertical wind shear. Similarly, the enhanced vertical wind shear over the low latitudinal region during opposite phases of ENSO/IOD. Climatologically, equatorial westerlies prevail in the lower troposphere, and easterlies stay in the upper troposphere during post-monsoon months (Fig. 6). Both the lower-level (850 hPa) westerlies and upper-level (200 hPa) easterlies weaken during El Niño and positive IOD years (Fig. 10), resulting in the weakening of the vertical wind shear. Similarly, the enhanced vertical wind shear is caused by the strengthening of anomalous lower-level westerlies and upper-level easterlies during La Niña and negative IOD years (Fig. 10).

We investigated the interannual variability of post-monsoonal cyclones, focusing on those formed in the low latitudes of the Bay of Bengal (BoB) and their teleconnection with El Niño Southern Oscillation (ENSO) and Indian Ocean Dipole (IOD). The main conclusions of this study are:

- (1) Post-monsoon LLC frequency in the BoB significantly decreases during El Niño and positive IOD years. In contrast, the La Niña and negative IOD years are associated with increased post-monsoon LLC frequency (Table 2, Figs. 2 and 7b). In ENSO years, the modulation in TC frequency is confined to the low latitudes only, with no change in HLC frequency. There are changes in HLC frequency during IOD years, but changes in LLC frequency still dominate.
- (2) The vital parameter responsible for the interannual variability in BoB LLCs was shown to be relative vorticity (Figs. 3i, j and 4i, j). The lower-tropospheric zonal winds determined this modulation in relative vorticity. The strong equatorial westerly winds in the Indian Ocean during the post-monsoon season create cyclonic circulation in the low latitudes of the BoB (Fig. 6) and build up sufficient absolute vorticity (Fig. 7a). During El Niño and positive IOD years, the climatological westerly winds in the equatorial Indian Ocean weaken (Figs. 7 and 8), which reduces the vorticity in the BoB (Figs. 3i, 4i and 7a). On the other hand, the strengthening of equatorial westerlies enhances the vorticity in the low latitudinal region of the BoB during La Niña and negative IOD (Figs. 3j, 4j and 7a) years. The weakening of relative vorticity significantly reduces the genesis of LLC (Fig. 7b). The relative vorticity-induced TC frequency reduction is confined to the LLC genesis region under a weak planetary vorticity environment. However, the TC frequency over the HLC genesis region was not significantly affected by the relative vorticity reduction under a stronger planetary vorticity environment. These results may help extend the lead time and improve the seasonal prediction of BoB TCs.

METHODS

The cyclone data from the Regional Specialized Meteorological Centre⁴³ is used to determine the genesis location and frequency of cyclones in the BoB during 1979–2020⁴⁴. The critical environmental parameters controlling cyclogenesis are obtained from the European Centre for Medium-Range Weather Forecasts (ECMWF)'s fifth-generation reanalysis dataset ERA5⁴⁵. To identify positive and negative phases of ENSO (El Niño/La Niña), we used the Oceanic El Niño Index²⁶. The Oceanic El Niño Index (ONI) is calculated as the three-month running mean of SST anomalies in the El Niño 3.4 region. It is obtained from the Climate Prediction Center, National Oceanic and Atmospheric Administration (NOAA, <http://www.cpc.ncep.noaa.gov>). We selected the El Niño (La Niña) years in which the index is greater than (less than) or equal to 0.5 °C (−0.5 °C) for a minimum of four consecutive overlapping seasons. The Dipole Mode Index (DMI) is used to identify the positive and negative phases of IOD²⁹. The DMI is defined as the difference in the SST anomalies between the western Indian Ocean (50°–70°E, 10°S–10°N) and the southeastern Indian Ocean (90°–110°E, 10°S–0°). The DMI index is taken from the NOAA's Physical Sciences Laboratory https://psl.noaa.gov/gcos_wgsp/Timeseries/DMI/. The tropical cyclone heat potential (TCHP) estimation is based on the ocean temperature data (EN4⁴⁶) obtained from the Met Office Hadley Centre. We used monthly data of different environmental parameters influencing TC formation for the composites of El Niño, La Niña, and IOD years based on October–December seasonal mean during 1979–2020.

DATA AVAILABILITY

All data used in this study are publicly available. The ERA5 reanalysis data are available to download from the <https://www.ecmwf.int/en/forecasts/datasets/reanalysis-datasets/era5>. The tracks and frequency of the north Indian Ocean cyclones used in this study are available on the archives of the India Meteorological Department (<https://rsmcnewdelhi.imd.gov.in>).

CODE AVAILABILITY

The codes for analysis, statistical computing, and graphics are based on freeware environments, R (version 4.0.5, <https://www.R-project.org/>), NCAR Command

Language (Version 6.6.2; <https://doi.org/10.5065/D6WD3XH5>), Ferret (version 7.5, <http://ferret.pmel.noaa.gov/Ferret/>) and CDO (version 1.9.2, <https://doi.org/10.5281/zenodo.3539275>). All codes developed to analyze the data are available at https://github.com/Shintoroose/NIO_LLC_interannual.

Received: 21 September 2021; Accepted: 22 March 2022;

Published online: 19 April 2022

REFERENCES

1. O'Hare, G. Hurricane 07B in the Godavari delta, Andhra Pradesh, India: vulnerability, mitigation and the spatial impact. *Geogr. J.* **167**, 23–38 (2001).
2. De, U., Dube, R. K. & Rao, G. P. Extreme weather events over India in the last 100 years. *J. Ind. Geophys. Union* **9**, 173–187 (2005).
3. Hoarau, K., Bernard, J. & Chalonge, L. Intense tropical cyclone activities in the northern Indian Ocean. *Int. J. Climatol.* **32**, 1935–1945 (2012).
4. Needham, H. F., Keim, B. D. & Sathiaraj, D. A review of tropical cyclone-generated storm surges: Global data sources, observations, and impacts. *Rev. Geophys.* **53**, 545–591 (2015).
5. Emanuel, K. Increasing destructiveness of tropical cyclones over the past 30 years. *Nature* **436**, 686–688 (2005).
6. Palmén, E. On the formation and structure of tropical hurricanes. *Geophysica* **3**, 26–38 (1948).
7. Fisher, E. L. Hurricanes and the sea-surface temperature field. *J. Atmos. Sci.* **15**, 328–333 (1958).
8. Gray, W. M. Global view of the origin of tropical disturbances and storms. *Mon. Weather Rev.* **96**, 669–700 (1968).
9. Gray, W. M. The formation of tropical cyclones. *Meteorol. Atmos. Phys.* **67**, 37–69 (1998).
10. Niyas, N., Srivastava, A. & Hatwar, H. Variability and trend in the cyclonic storms over north Indian Ocean. Met Monograph: Cyclonic Warning-3 (India Meteorological Department, 2009).
11. Krishnamurthy, V. & Ajayamohan, R. S. Composite structure of monsoon low pressure systems and its relation to Indian rainfall. *J. Climate* **23**, 4825–4305 (2010).
12. Alam, M. M., Hossain, M. A. & Shafee, S. Frequency of Bay of Bengal cyclonic storms and depressions crossing different coastal zones. *Int. J. Climatol.* **23**, 1119–1125 (2003).
13. Mohapatra, M., Bandyopadhyay, B. & Tyagi, A. Best track parameters of tropical cyclones over the north Indian Ocean: a review. *Nat. Hazards* **63**, 1285–1317 (2012).
14. Webster, P. J., Holland, G. J., Curry, J. A. & Chang, H. R. Changes in tropical cyclone number, duration, and intensity in a warming environment. *Science* **309**, 1844–1846 (2005).
15. Rao, S. A. et al. Why is Indian Ocean warming consistently? *Clim. Change* **110**, 709–719 (2012).
16. Kumar, P. D., Paul, Y. S., Muraleedharan, K., Murty, V. & Preenu, P. Comparison of long-term variability of sea surface temperature in the Arabian Sea and Bay of Bengal. *Reg. Stud. Mar. Sci.* **3**, 67–75 (2016).
17. Roxy, M. K., Ritika, K., Terray, P. & Masson, S. The curious case of Indian Ocean warming. *J. Climate* **27**, 8501–8509 (2014).
18. Bhardwaj, P. & Singh, O. Trends in frequency and intensity of tropical cyclones in the Bay of Bengal: 1972–2015. In *Basics of Computational Geophysics*, 389–397 (Elsevier, 2021).
19. Deshpande, M. et al. Changing status of tropical cyclones over the north Indian Ocean. *Clim. Dyn.* **57**, 3545–3567 (2021).
20. Knutson, T. R. et al. Tropical cyclones and climate change. *Nat. Geosci.* **3**, 157–163 (2010).
21. Mittal, R. et al. Response of tropical cyclone Phailin (2013) in the Bay of Bengal to climate perturbations. *Clim. Dynam.* **53**, 2013–2030 (2019).
22. Balaguru, K., Taraphdar, S., Leung, L. R. & Foltz, G. R. Increase in the intensity of post-monsoon Bay of Bengal tropical cyclones. *Geophys. Res. Lett.* **41**, 3594–3601 (2014).
23. Balaji, M., Chakraborty, A. & Mandal, M. Changes in tropical cyclone activity in north Indian ocean during satellite era (1981–2014). *Int. J. Climatol.* **38**, 2819–2837 (2018).
24. Sahoo, B. & Bhaskaran, P. K. Assessment on historical cyclone tracks in the Bay of Bengal, east coast of India. *Int. J. Climatol.* **36**, 95–109 (2016).
25. Pan, Y. H. & Oort, A. H. Global climate variations connected with sea surface temperature anomalies in the eastern equatorial Pacific Ocean for the 1958–73 period. *Mon. Weather Rev.* **111**, 1244–1258 (1983).
26. Trenberth, K. E. The definition of El Niño. *Bull. Amer. Meteorol. Soc.* **78**, 2771–2778 (1997).

27. McPhaden, M. J. El Niño and la niña: causes and global consequences. In MacCracken, M. & Perry, J. (eds.) *Encyclopedia of Global Environmental Change*, vol. 1 of series *The Earth System: Physical and Chemical Dimensions of Global Environmental Change*. 353–370 (John Wiley and Sons, LTD., Chichester, UK; 2002).
28. Walker, S. G. T. & Bliss, E. W. World weather VI. *Mem. Roy. Meteorol. Soc.* **4**, 119–139 (1937).
29. Saji, N. H., Goswami, B. N., Vinayachandran, P. & Yamagata, T. A dipole mode in the tropical Indian ocean. *Nature* **401**, 360–363 (1999).
30. Camargo, S. J., Emanuel, K. A. & Sobel, A. H. Use of a genesis potential index to diagnose ENSO effects on tropical cyclone genesis. *J. Clim.* **20**, 4819–4834 (2007).
31. Girishkumar, M. S. & Ravichandran, M. The influences of ENSO on tropical cyclone activity in the Bay of Bengal during October–December. *J. Geophys. Res.* **117**, 1–13 (2012).
32. Felton, C. S., Subrahmanyam, B. & Murty, V. ENSO-modulated cyclogenesis over the Bay of Bengal. *J. Clim.* **26**, 9806–9818 (2013).
33. Yuan, J. & Cao, J. North Indian Ocean tropical cyclone activities influenced by the Indian Ocean Dipole mode. *Sci. China Earth Sci.* **56**, 855–865 (2013).
34. Mahala, B. K., Nayak, B. K. & Mohanty, P. K. Impacts of ENSO and IOD on tropical cyclone activity in the Bay of Bengal. *Nat. Hazards* **75**, 1105–1125 (2015).
35. Leipper, D. F. & Volgenau, D. Hurricane heat potential of the Gulf of Mexico. *J. Phys. Oceanogr.* **2**, 218–224 (1972).
36. Thomas, A., Samala, B. K. & Kaginalkar, A. Simulation of north Indian Ocean tropical cyclones using RAMS numerical weather prediction model. *Trop. Cyclone Res. Rev.* **3**, 44–52 (2014).
37. Paterson, L. A., Hanstrum, B. N., Davidson, N. E. & Weber, H. C. Influence of environmental vertical wind shear on the intensity of hurricane-strength tropical cyclones in the Australian region. *Mon. Weather Rev.* **133**, 3644–3660 (2005).
38. Roose, S. et al. Pacific decadal oscillation causes fewer near-equatorial cyclones in North Indian Ocean Preprint available at <https://doi.org/10.21203/rs.3.rs-566899/v1> (2021).
39. Bister, M. Effect of peripheral convection on tropical cyclone formation. *J. Atmos. Sci.* **58**, 3463–3476 (2001).
40. Li, T., Ge, X., Peng, M. & Wang, W. Dependence of tropical cyclone intensification on the Coriolis parameter. *Trop. Cyclone Res. Rev.* **2**, 1–12 (2012).
41. DeMaria, M. & Pickle, J. D. A simplified system of equations for simulation of tropical cyclones. *J. Atmos. Sci.* **45**, 1542–1554 (1988).
42. Schreck, C. J., Molinari, J. & Mohr, K. I. Attributing tropical cyclogenesis to equatorial waves in the western north Pacific. *J. Atmos. Sci.* **68**, 195–209 (2011).
43. RSMC. Report on cyclonic disturbances over the north Indian Ocean during 2017. Tech. Rep., India Meteorological Department, New Delhi (2018). Available at <http://www.rsmcnewdelhi.imd.gov.in/images/pdf/publications/annual-rsmc-report/RSMC-2017.pdf>.
44. Cyclone-eAtlas. Tracks of cyclones and depressions over north Indian Ocean. Version, (2011). Available at <http://www.rmccennaieatlas.tn.nic.in>
45. Hersbach, H. et al. The ERA5 global reanalysis. *Quart. J. Roy. Meteorol. Soc.* **146**, 1999–2049 (2020).
46. Good, S. A., Martin, M. J. & Rayner, N. A. EN4: Quality controlled ocean temperature and salinity profiles and monthly objective analyses with uncertainty estimates. *J. Geophys. Res.* **118**, 6704–6716 (2013).

ACKNOWLEDGEMENTS

The Center for Prototype Climate Modeling is fully supported by the Abu Dhabi Government through New York University Abu Dhabi Research Institute Grant. RSA was supported by Tamkeen through research grant CG009 to NYUAD's ACCESS research center. This work was also supported by the Monsoon Mission project of the Ministry of Earth Sciences, Government of India (Grant No. MM/SERP/NYU/2014/SSC-01/002) to RSA, and the Office of Naval Research (ONR, N00014-1601-3091) to P.R. The authors thank Dr. Roxy Mathew Koll and Vineet Kumar Singh for sharing codes to remove TC-related anomalies from the basic flow.

AUTHOR CONTRIBUTIONS

S.R., R.S.A., and P.R. conceived the idea and proposed this study. All the authors discussed the concepts and the methodology. The manuscript was drafted by S.R. and edited by all authors.

COMPETING INTERESTS

The authors declare no competing interests.

ADDITIONAL INFORMATION

Supplementary information The online version contains supplementary material available at <https://doi.org/10.1038/s41612-022-00252-8>.

Correspondence and requests for materials should be addressed to R. S. Ajayamohan.

Reprints and permission information is available at <http://www.nature.com/reprints>

Publisher's note Springer Nature remains neutral with regard to jurisdictional claims in published maps and institutional affiliations.



Open Access This article is licensed under a Creative Commons Attribution 4.0 International License, which permits use, sharing, adaptation, distribution and reproduction in any medium or format, as long as you give appropriate credit to the original author(s) and the source, provide a link to the Creative Commons license, and indicate if changes were made. The images or other third party material in this article are included in the article's Creative Commons license, unless indicated otherwise in a credit line to the material. If material is not included in the article's Creative Commons license and your intended use is not permitted by statutory regulation or exceeds the permitted use, you will need to obtain permission directly from the copyright holder. To view a copy of this license, visit <http://creativecommons.org/licenses/by/4.0/>.

© The Author(s) 2022